RESEARCH ARTICLE OPEN ACCESS

Electrochemical Behavior of Nitrofurazone in Aqueous Media Applying Multi-Walled Carbon Nanotubes and Cu-Phthalocyanine

Charles L. Brito[1] 🆔 | Elizabeth I. Ferreira[1] | Mauro A. La-Scalea[2]

[1]Department of Pharmacy, Faculty of Pharmaceutical Sciences, University of São Paulo, São Paulo, Brasil | [2]Department of Chemistry, Institute of Environmental, Chemical and Pharmaceutical Sciences, Federal University of São Paulo, Diadema, Brasil

Correspondence: Charles L. Brito (charles.brito@usp.br) | Mauro A. La-Scalea (mauro.scalea@unifesp.br)

ABSTRACT

A copper phthalocyanine (CuPc) and functionalization multi-walled carbon nanotubes with carboxylic acids groups (C-MWCNTs) modified glassy carbon electrode and was used to evaluate the electrochemical behavior of nitrofurazone (NF). The modification of the glassy carbon electrode (GCE) increased the cathodic current response related to hydroxylamine derivative in acid media and promoted electrocatalytic process with 107 mV potential anticipation, when compared to the bare GCE. Furthermore, from pH > 9, the NF reduction appeared at the potential peak, which anticipated the hydroxylamine derivative. This peak was associated to the nitro-anion radical derivative formation in one-electron reversible process. The reduction potential of radical was anticipated in 290 mV and the peak currents were approximately 10 times higher than the bare GCE. In addition to that, this radical presented a lifetime twice more stable compared to bare GCE. The molecular O_2 was confirmed as the best radical scavenger instead of glutathione and cysteine one. Therefore, the advantages of combining CuPc with C-MWCNT in improving the detection properties of reduction intermediates from nitrofurazone have been presented, being an innovative, sensitive, reproducible method that can be a useful tool for other nitroheterocyclic purposes to obtain lifetime of radical and relate it to antichagasic activity.

1 | Introduction

The comprehension of the reduction mechanism of nitroheterocyclic compounds is relevant to know the parameters, which can establish the correlation between electron transfer and biological activity. Nitrofurazone (NF), a drug containing the 5-nitroheterocyclic moiety (Figure 1), is active against *Trypanosoma cruzi*, which is the etiologic agent of Chagas disease. Data from the literature indicate that nitroheterocyclic derivatives act as trypanothione reductase (TR) substrates and are also effective enzymatic inhibitors of the reduction of

trypanothione disulfide—physiological substrate of this enzyme [1, 2]. Furthermore, it is noted that these intermediates are formed from the reduction reaction of these drugs and can also cause damage to the enzymes and DNA of *T. cruzi* [3–5]. Therefore, the process of reduction of nitroheterocyclic and the formation of the nitro-anion radical, R-NO$_2$$^{\bullet-}$, is considered a fundamental step for biological activity [6–8].

The reduction of nitroheterocyclic is a complex process and can be carried out through two different mechanisms according to whether the medium is anaerobic or aerobic, being in both
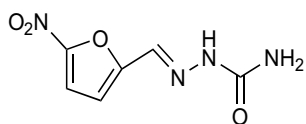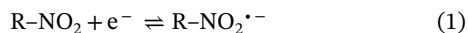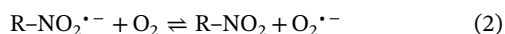
FIGURE 1 | Structure of nitrofurazone (NF).

conditions; the first step is the reduction of an electron to form the nitro radical anion [6–8].

$$R{-}NO_2 + e^- \rightleftharpoons R{-}NO_2^{\bullet -} \qquad (1)$$

In the anaerobic metabolic pathway, the nitro-anion radical generated is transformed into a nitroso derivative (ArNO) and, in sequence, the hydroxylamine derivative (ArNHOH) is formed, followed by the amine derivative (ArNH$_2$) formation [6–8]. Thus, these intermediates production involves the transfer of two, four and six electrons, respectively. Nevertheless, under aerobic conditions, the initial nitro compound is regenerated by the nitro-anion radical re-oxidation producing superoxide (O$_2^{\bullet -}$), as follows [6–8]:

$$R{-}NO_2^{\bullet -} + O_2 \rightleftharpoons R{-}NO_2 + O_2^{\bullet -} \qquad (2)$$

This anion will form hydrogen peroxide, either spontaneously or under the catalytic effect of the enzyme superoxide dismutase (SOD) [6–8].

Several results in the literature [6–10] show that the electrochemical generation and stabilization of nitro-anion radical may be related to the characteristics of the working electrode material, as well as to the process of treatment/activation of its surface. It is classically known that adsorption phenomena interfere with this stability, which increases its half-life by suppressing the protonation of the radical in the diffusion layer [6–8]. Classically, electrochemical studies on the mechanism of nitrocompounds reduction are performed by means of cyclic voltammetry (CV) [9, 10].

The detection of R-NO$_2^{\bullet -}$, from the electrochemical reduction process through CV are well known in solid electrodes, but its reduction occurs at a relatively high potential in conventional carbon electrodes. Consequently, considerable effort has been devoted toward the identification of new electrode materials that will reduce the overpotential for nitroheterocyclic compound reduction. Chemically modified carbon electrode containing metallic complexes, highlighting the phthalocyanines of Fe (II), Cu (II) (Figure 2A), and Co (II), Mn (II), are recognized

FIGURE 2 | (A) Chemical structure of copper phthalocyanine (CuPc), (B) chemical structure of iron protoporphyrin IX.

as agents that catalyze a variety of redox reactions. These complexes are recognized for their excellent electrocatalytic activity in many reactions, which are dependent on the central atom [11–13]. Phthalocyanines (Pc) were discovered in the early 20th century by Brun and Tcherniac in London, corresponding to a byproduct of the synthesis of o-cyanobenzamide, using phthalamide and acetic anhydride as starting materials [14, 15]. These materials are structurally similar to porphyrins, as they have planar macrocyclic groups, with the presence of 18 pairs of π electrons, delocalized. This electronic arrangement conditions their main properties, such as chemical and thermal stability areas [14–16]. Phthalocyanines are similar to P450 enzymes, from the oxidoreductase family, which act on various xenobiotics and drugs. In general, P450 enzymes have an active site that is common to all of them, ferriprotoporphyrin IX (Figure 2B) [17, 18].

There are few works focused on modifying the electrode surface for studies to identify reduction intermediates of nitroheterocyclic compounds using Cu complexes, mimetizing nitroreductases such as that recorded for metronidazole, combining the concept of molecularly imprinted polymer (MIP) [19]. Copper (II) and iron (III) metal complexes [20] are essential to life and are the transition metals considered essential for the maintenance of life and are also the most concentrated in all living organisms, acting for example as transport proteins such as ceruloplasmin (copper) and transferrin (iron) [20]. Recent studies show the development of methods using glassy carbon electrodes, with copper II germanate nanowire [21] for substrate modification and subsequent determination of tartaric acid. The fact that this acid is not electroactive in conventional electrodes makes the development of voltammetric methods for determining this acid scarce, thus imposing the need to use modified electrodes for the development of such analysis methods.

CuPc was discovered almost 80 years ago, and few electrochemical studies can be found in the literature [22–24]. The studies demonstrated that the metal center does not participate in the reaction; in this case, the oxidation and/or reduction reactions occur only in the Pc ring [24]. It is well established in the literature that CuPc presents reversible redox processes in which the observed signals, both in the anodic and cathodic ranges, were attributed to the electroactivity of the Pc rings [24].

In the current article, we outline a rapid procedure for creating an electrode that has been modified using copper (II) and multi-walled carbon nanotubes (MWCNTs). The C-MWCNT combined with CuPc on GCE modified was utilized for behavior voltammetric investigation nitrofurazone.

Due to the attractive characteristics of C-MWCNT and CuPc, the reduction of nitrofurazone can be greatly improved, and its cathodic peak currents, mainly of R-NO$_2^{\bullet -}$ formation, can be significantly increased and at low concentrations compared to other works of the same scope.

Despite these advances, few studies integrate CuPc with carbon nanomaterials for nitroheterocyclic analysis. Prior work on metronidazole [19] and tartaric acid [21] highlights the potential of Cu-based modifiers to mimic nitroreductases and lower detection limits. Here, we bridge this gap by developing a glassy carbon
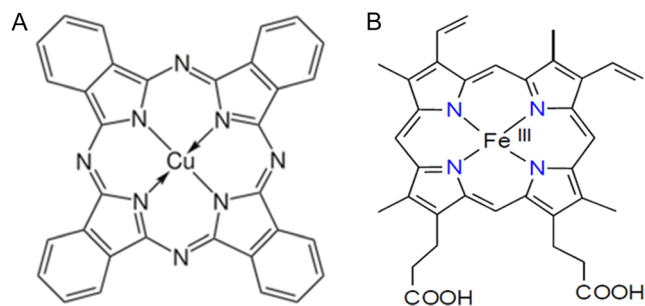
electrode (GCE) modified with CuPc and C-MWCNTs to investigate NF's redox behavior. By stabilizing reactive intermediates and elucidating their decay pathways, this platform advances the electrochemical profiling of nitroheterocyclic drugs. The methodology's reproducibility and sensitivity (sub-µM detection) position it as a transformative tool for linking radical dynamics to antichagasic activity, offering insights for rational drug design and quality control.

2 | Experimental Section

2.1 | Chemicals

(a) Phosphate buffer stock solutions $2.01 \leq pH \leq 10.04$ [25]: Phosphate buffer stock solutions were prepared from the mixture NaH_2PO_4 (monobasic sodium phosphate) and Na_2HPO_4 (dibasic sodium phosphate) to 100 mL of ultrapure water. To adjust the pH, solutions of sodium hydroxide, NaOH 2.0 mol L^{-1}, were used for pH above 7.0, and phosphoric acid, H_3PO_4 p.a., for values below 7.0. The final pH of each buffer solution was measured with a combined glass electrode connected to a Metrohm pH-measuring device, model 744, at room temperature.

(b) 1.0 mmol L^{-1} stock solution of NF: The stock solution of the analyte was prepared by directly dissolving appropriate amount of the NF in a mixture (1 : 1) of N, N-dimethylformamide (DMF) and ultrapure water with the aid of ultrasound (40 KHz). The solution obtained was stored in an amber bottle, to avoid photochemical degradation, and subsequently stored at room temperature for a maximum of 1 month.

(c) Stock solution of 3.5×10^{-2} mol L^{-1} of cysteine and glutathione: solutions were prepared by dissolving in appropriate amount of L-cysteine and (Cys) and glutathione (GSH) in ultrapure water (Arotec).

2.2 | Electrochemical Instruments

Cyclic voltammograms were recorded using the potentiostat/galvanostat Methrom Autolab PGSTAT 30, Eco-Chimie, coupled to an electrochemistry cell with three electrodes: bare/modified glassy carbon as working electrode, Ag/AgCl as reference and Pt as auxiliary electrode. The OriginLabTM program version 8.0 was used for data processing. All experiments were conducted at room temperature, electrochemical cell with a volume of 20 mL and it was deareted by passing nitrogen gas.

2.3 | Procedures

a) Treatment of glassy carbon electrode and GCE modified by C-MWCNT combined with CuPc (from Sigma–Aldrich). The glassy carbon electrode (GCE, Ø = 2 mm) was manually polished with alumina suspension (Arotec) particle size 0.3 µm on metallographic felt for polishing type DBM (Arotec) and then washed thoroughly with purified water. After this procedure, the GCE was placed in buffer solution and potentials of 1.0 and −1.0 V were applied for 10 s each, followed by a potential sweep between

0 and −1.0 V until establishing a constant baseline. The glassy carbon electrode was modified by C-MWCNT combined with CuPc, being MWCNTs functionalized and characterized with insertion of acid carboxylic groups according to the previous reports following the method published [26]. Dispersion in the ratio of 3 : 1 between C-MWCNT with CuPc was established using 1,3-dioxolane as solvent by different time intervals $1 \leq t \leq 18$ min ultrasonic agitation of 40 KHz for a homogeneous dispersion. This electrode was left at room temperature until complete drying of the applied solution and then washed with purified water to remove the excess mixture between C-MWCNT and CuPc adsorbed on the surface of glassy carbon. Calculation of the active area of the GCE (0.0144 cm^2) and GCE-C-MWCNT (0.136 cm^2) sensor followed the protocol previously published elsewhere [26, 27].

b) Morphological and spectrometric characterization of the dispersion. The images of the dispersions between C-MWCNT with CuPc were obtained using Jeol equipment model JSM-6610 LV, with the samples being dispersed in methanol, treated in ultrasound for 15 min, applied to the surface of double-sided copper tape previously glued to the sample holder and then dried under reduced pressure and metalized with gold. The acceleration voltage was 30 to 0.1 KV, resolution 0.5 µm (15 KV) and maximum magnification: 25,000 times. The appearance and disappearance of bands in the dispersion of C-MWCNT with CuPc were compared with the bands obtained from CuPc isolated by means of attenuated total reflectance (ATR) mode, in Shimadzu IR Affinity-1. These samples were placed in a desiccator for 24 hr and scans were performed in the region from 400 to 4000 cm^{-1}, being each spectrum accumulated 60 times at 4 cm^{-1} of resolution.

c) Stability of GCE modified by C-MWCNT combined with CuPc. The stability of the sensor was evaluated by measuring the current peak for voltammograms recorded in a 0.1 mmol L^{-1} NF solution in phosphate buffer pH 4.02, in which 56 measurements were carried out for 11 days and the sensor was cleaned by washing deionized water treatments. Furthermore, the electrode was kept inside the desiccator, having silica as dehumidifying agent in a vertical position supported on a styrofoam plate.

d) Interaction between radical scavengers and nitro radical anion in C-MWCNT combined with CuPc. This interaction between nitro radical anion from NF with Cys, GSH and molecular oxygen (O_2) was analyzed by CV in an electrochemical cell containing 0.1 mmol L^{-1} NF in phosphate buffer pH 9.05 and deareted for 15 min with nitrogen gas, N_2. For the use of GSH and Cys, adequate volumes of a 3.5×10^{-2} mol L^{-1} stock solution of Cys and GSH were used. On the contrary, the studies used molecular oxygen, with a flow of 1 mL min^{-1} at time intervals of 5 and 10 min. After each new reading with O_2 at studied time intervals, O_2 was purged again from the cell.

e) Determination of rate constants. Employing the model of the current ratio, Ipa/Ipc, values were measured at each scan rate, being: $I_{pa}/I_{pc} = I_{pa_0}/I_{pc_0} + 0.485 \ I_\lambda/I_{pc_0} + 0.086$, with I_{pa_0} = the anodic peak current due to zero current; I_{pc_0} = the cathodic peak current due to zero current and I_λ the current measured at the

inversion potential [28]. A working curve used was the fit equation $y = 0.0116x^2 - 0.1239x + 0.995$ ($R = 0.999$) and plotted, in which $y = I_{pa}/I_{pc}$ and $x = \varpi$ [29], whose ϖ parameter incorporates the effects of rate constant, drug concentration, and scan rate. Considering planar electrode for the condition $a\tau = 4$, the ϖ versus results in a linear relationship can be described by the equation $\varpi = k_2 C\tau$, in which k_2 is the rate constant value for the second-order reaction for the nitro radical anion decay obtained from this plot slope. The parameter C is the drug concentration and $\tau = (E_{1/2}-E_\lambda)/\nu$, in which $E_{1/2} = E_{pc} + 0.0285/n$, being E_{pc} the peak potential, n the number of electrons, E_λ is the potential of inversion in cyclic voltammetry and ν scan rate. The nitro-anion radical stability was calculated by the half-time life equation $t_{1/2} = 1/[\text{R-NO}_2^{\bullet-}] \, k_2$, assuming that $[\text{R-NO}_2^{\bullet-}]$ = drug concentration.

3 | Results and Discussion

3.1 | The Characterization of Multi-Walled Carbon Nanotubes with CuPc

Scanning electron microscopy (SEM) analysis (Figure 3A) revealed heterogeneous CuPc agglomerates on the C-MWCNT surface, exhibiting distinct cylindrical and rounded morphologies (upper right and central regions, respectively). Such aggregation—common in metal complexes like CuPc—arises from dimer/trimer formation and higher-order stacking, which detrimentally impacts quantum yield and electron transport efficiency by hindering charge transfer pathways [30, 31]. Notably, CuPc aggregates here displayed less uniformity and larger sizes compared to prior work with hemin [27], where smaller, more homogeneous structures suggested stronger interactions with C-MWCNTs.

C-MWCNTs retained their characteristic thread-like organization, but CuPc's irregular aggregation highlights weaker interfacial synergy than observed with hemin. Complementary FTIR studies were conducted to probe chemical interactions between CuPc's functional groups and C-MWCNTs, providing insights into the composite's electronic and structural behavior. These findings underscore the need to optimize CuPc dispersion to enhance electron transport in catalytic applications. For this, the ATR system interface was used, comparing the spectra of CuPc and C-MWCNT combined with CuPc as shown in Figure 3B. These FTIR signal assignments are presented on Table 1. The band at 1334 cm^{-1} recorded by the CuPc complex was related to the stretch of the pyrroline group, being absent when combined with C-MWCNT. Furthermore, a characteristic band stands out at 1417 cm^{-1} for CuPc due to the stretching of the nitrogen of the isoindolic group, which disappeared in the presence of C-MWCNT [33]. This effect may indicate a possible point of interaction between the metallic complexes and the C-MWCNT, due to the hydrogen bond between the nitrogens, pyrrolinic, or indolic, with the hydrogen present in the carboxylic groups of C-MWCNT. Moreover, it is important to note that at 1020 cm^{-1} the corresponding signal of the interaction between the metallic center and the ring in CuPc disappeared when this complex combined with C-MWCNT, indicating another possible point of electrostatic interaction between Cu and the carboxylic groups of C-MWCNT [32].

In a complementary way, a 705 cm^{-1} band, which refers to the perpendicular orientation of the CuPc to the plane, was affected and suppressed in the presence of C-MWCNT, beyond recording an increase in the intensity of the bands 3740, 151, and 1525 cm^{-1}, which are related, respectively, to the N-H, C=O from

TABLE 1 | Attribution of the main differences between the FTIR bands for isolated CuPc and C-MWCNT combined with CuPc.

$\cong$ Wave number (cm^{-1})	CuPc	C-MWCNT-CuPc	Assignment [32]
3740	+	++	ν N-H of amino group
1751	+	++	ν C=O of carboxylic acid
1525	+	++	ν (-N=)
117	++	–	ν (-N=), isoindole
1334	++	–	ν (-N=) pyrrol
1020	++	–	δ (M-macrocycle)
705	++	–	δ (C–H) perpendicular to the plane

Note: (++): sign increase, (+): presence of sign, (−) absence of sign, (ν): stretch and (δ): deformation.
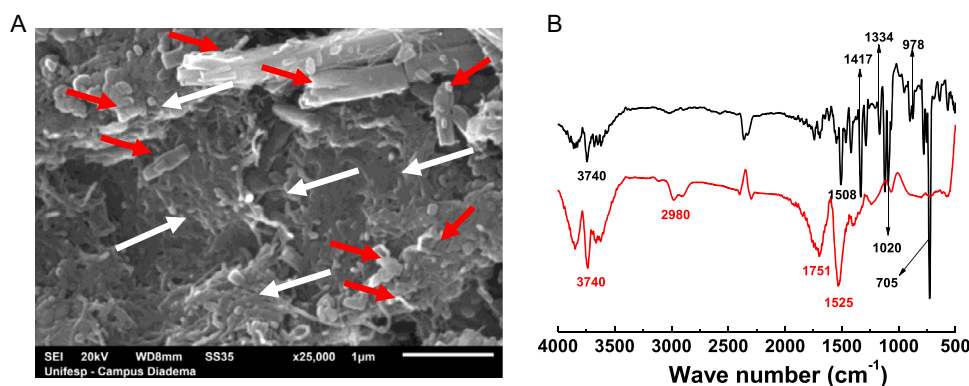

FIGURE 3 | (A) Scanning electron microscopy (SEM): CuPc is marked in red arrow and C-MWCNT is marked in white arrow, wire format. (B) Comparative spectra of absorption in the infrared region between CuPc (black) and C-MWCNT-CuPc (red).

carboxylic acid and -N= stretches. These increased band intensities can be attributed to the contribution of the vibrational mode due to electronic resonance effects [32]. The FTIR results corroborate the studies developed by Li et al. [33], who used X-ray photoelectronic spectroscopy (XPS) techniques and identified points of interaction between C-MWCNT and phthalocyanines. This work indicated that interactions occur between the metallic nucleus of phthalocyanine and the carboxyl group of C-MWCNT, as well as between the acidic hydrogen of C-MWCNT and the nitrogen of the amine groups of phthalocyanine through hydrogen bonding.

3.2 | Electrochemical Characterization of the Sensor Response and the Parameter Optimization

Modifying agents were dispersed in 1,3-dioxolane and their deposition on the GCE surface was carried out by drop casting method. The interaction of modifying materials with the electrode surface, especially when nanostructured carbon materials are used, is due to Van der Waals interactions. The cyclic voltammogram registered at acid media (pH 4.02) of NF on a GCE modified with C-MWNTC combined with CuPc complex was plotted comparatively with bare GCE and GCE modified with C-MWCNT-F (Figure 4A–C). The GCE-C-MWCNT-CuPc recorded only a single reduction wave ($E_{pc,1}$) and it was similar bare GCE and GCE-C-MWCNT. The sensor with CuPc presented less negative potential values (−0.328 V) and the higher current value, clearly indicating an electrocatalytic effect with a potential anticipation of 107 mV, compared to bare GCE (−0.435 V); and similar to the GCE-C-MWCNT (−0.335 V). It is worth mentioning that in this experimental conditions non-appearance of any signal related to copper, probably for the following two reasons: one that reinforces the proposed interaction between C-MWCNT and CuPc, which inhibits the appearance of CuPc reduction in the region between −0.95 and −1.0 V and the other reason is that the appearance of the signal of CuPc maybe given at values more negative than −1.0 V, but the potential working range of this article was $0.35 \leq E \leq -1.0$ V.

In addition, it was evident that the cathodic current value ($I_{pc,1}$) obtained with the sensor in the presence of the metal complex,

CuPc, has a significantly higher magnitude (32 and 1.5 times greater) than the bare sensor GCE and GCE-C-MWCNT, respectively. These results are compatible with those published using hemin as modifying agent with C-MWCNT on surface GCE [27]. This demonstrates that the use of both CuPc and hemin contributed to the anticipation of potential and to the increase in peak current. The cathodic peak ($E_{pc,1}$) corresponds to the nitro group reduction to the hydroxylamine derivative in a four-proton and four-electron process (Reaction 3), while the anodic peak ($E_{pa,1}$) refers to the oxidation of RNHOH to the R-NO derivative ($E_{pa,1} \cong + 0.16$ V).

$$R–NO_2 + 4e + 4H^+ \rightarrow R–NHOH + H_2O \qquad (3)$$

The ultrasound is the common procedure employed in dispersion between CNT with other chemical groups in a suspension employing organic solvent. This tool exceeds the numerous interactions of van der Waals between the CNT, which is interrupted by the shear force promoted by the cavitation effects [34]. The cyclic voltammograms indicate the influence of dispersion time (intervals of $1 \leq t \leq 18$ min) by ultrasonic bath at pH 4.02 for GCE-C-MWCNT-CuPc for NF, Figure 5A–D. It is possible to observe that the highest $I_{pc,1}$ value is obtained with dispersion time of 15 min, being that peak intensity, $I_{pc,1}$, suddenly increased between 1 and 5 min intervals to a smaller scale from 5 to 15 min. However, from this dispersion interval (18 min) there is a decrease in $I_{pc,1}$, in which the magnitude of the peak is similar to the result observed in 5 min, due to interval of more than 15 min, generating more defects in the MWCNT and impairing the transfer of electrons. Furthermore, the sensor lifetime is evaluated through CV obtained from the NF reduction process in acidic medium (pH 4.02) over different days with 5 readings and performed each day, being the sensor lifetime responses monitored for 11 days (Table 2).

3.3 | Nitrofurazone Voltammetry Behavior using Sensor GCE by C-MWCNT Combined with CuPc

Cyclic voltammetry experiments were carried out in phosphate buffer ($2.03 \leq pH \leq 6.06$) containing 0.1 mmol L^{-1} of NF and
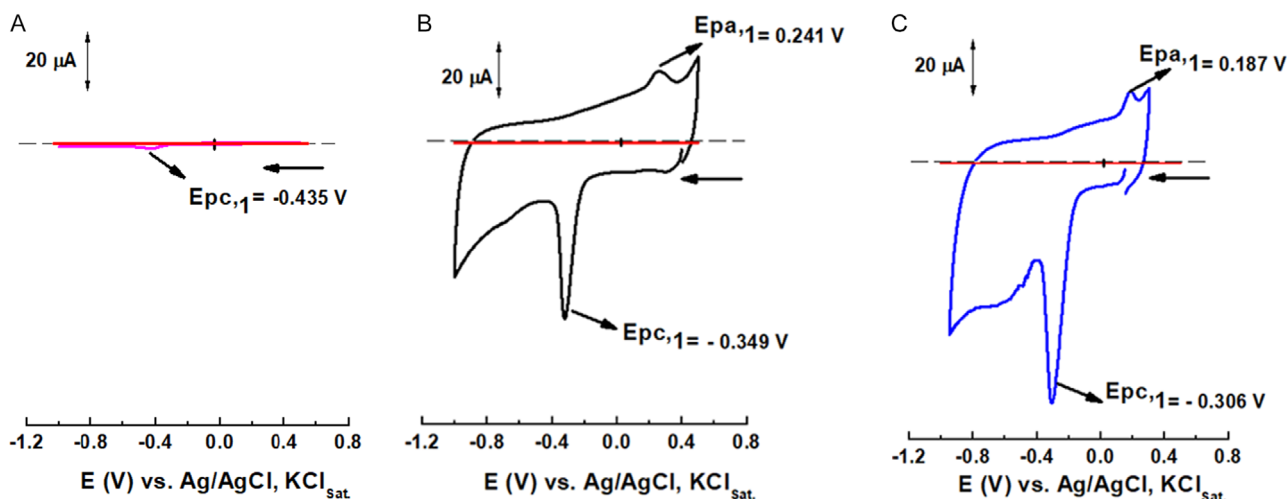

FIGURE 4 | Cyclic voltammograms recorded at pH 4.02, being blank (red). (A) (magenta) bare GCE, (B) (black) GCE-C-MWCNT and (C) (blue) GCE modified by C-MWCNT combined with CuPc [NF] = 0.1 mmol L^{-1} using CV and at ν = 200 mV s^{-1} (1st cycle).
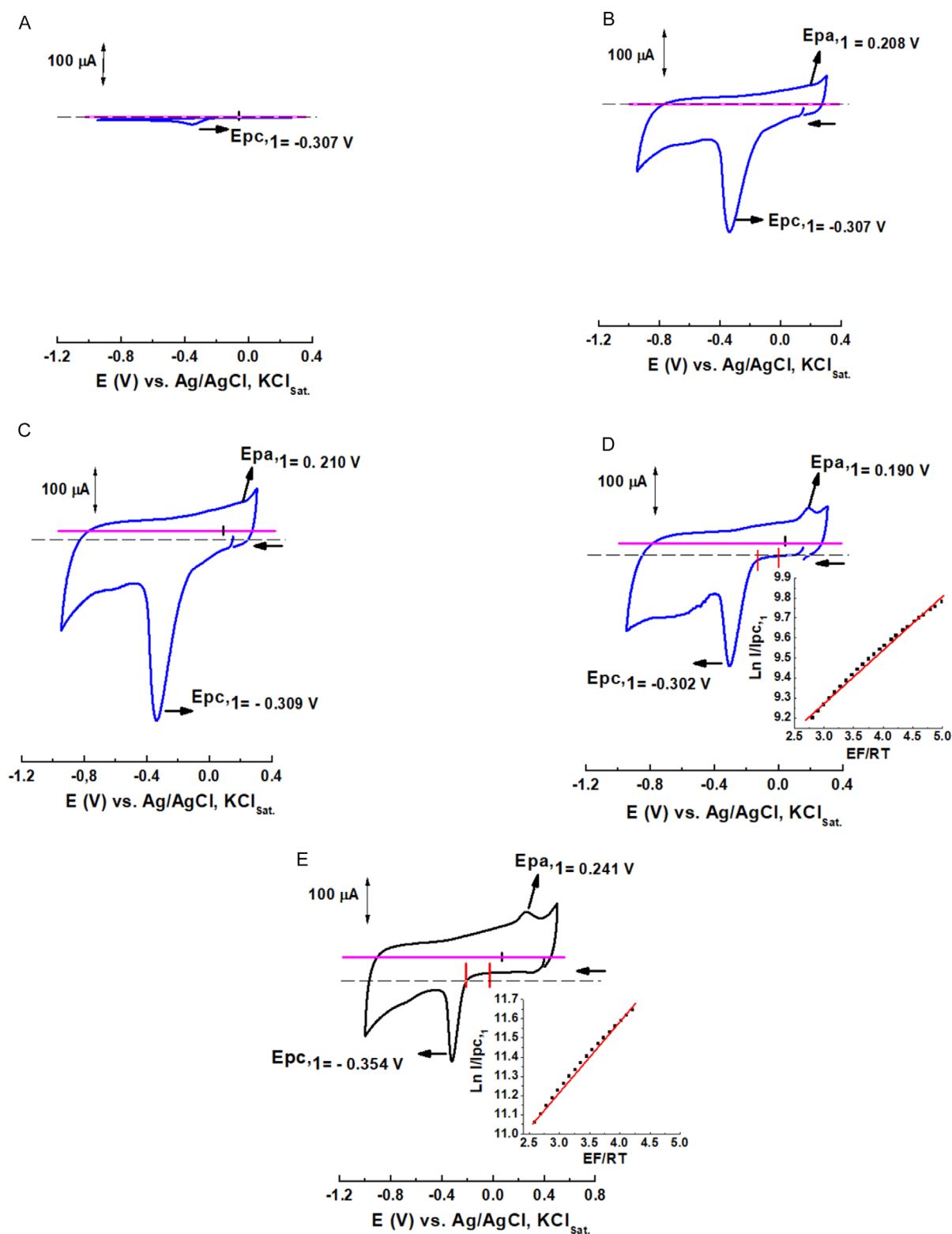
FIGURE 5 | Cyclic voltammograms recorded at pH 4.02, being blank (magenta) and (blue) GCE modified by C-MWCNT combined with CuPc (1st cycle), in ultrasound time intervals of $1 \leq t \leq 18$ min, being: (A) 1, (B) 5, (C) 15, and (D) 18 min. GCE modified by C-MWCNT, being blank (magenta) and black (E) 18 min. [NF] = 0.1 mmol L^{-1} using CV and at ν = 200 mV s^{-1}. Inset: the Tafel linear correlation referred to the potential range marked by the red bars (D and E).

scan rate of 200 mVs^{-1}. A well-defined reduction peak was observed for $E_{pc,1}$ and shifted to more negative potential values with increased pH, using bare GCE and GCE-C-MWCNT-CuPc as well. The latter sensor showed an anticipation of 80 mV

potential across the entire pH range studied for $E_{pc,1}$ and current increase of 40 times (Table 3). $E_{pc,1}$ value varied linearly with increasing pH, being the respective slope $\Delta E_{pc,1}/\Delta pH$ for the GCE-C-MWCNT-CuPc of 33 mV/pH. In previous study [27],

TABLE 2 | Values refer to $I_{pc,1}$ of obtained in the GCE modified by C-MWCNT combined with CuPc sensor in a period of 11 days, with 56 readings obtained, being this experiment realized in triplicate.

Readings	$I_{pc,1}$ (μA)	Drop of $I_{pc,1}$ in relation the read first (%)
1 a 20	47 ± 3	—
21 a 42	39 ± 4	17.02
43 a 50	30 ± 3	36.20
51 a 56	21 ± 2	55.40

TABLE 3 | Peak potential values, ($E_{pc,1}$) and ($I_{pc,1}$) in NF 0.1 mmol L−1 in 2.03 ≤ pH ≤ 6.06 for GCE modified by C-MWCNT combined with CuPc and bare GCE.

	GCE modified by C-MWCNT combined with CuPc		Bare GCE	
pH	$-E_{c,p1}$ (V)	$-I_{pc,1}$ (μA)	$-E_{c,p1}$ (V)	$-I_{pc,1}$ (μA)
2.03	0.293	35	0.358	1.0
3.03	0.301	37	0.401	1.0
4.02	0.302	45	0.435	1.5
5.02	0.385	46	0.461	0.8
6.06	0.413	40	0.501	1.0

this slope was similar when combined with C-MWCNT and C-MWCNT-HEM presenting 36 and 39 mV/pH, respectively.

Based on these results, it is observed that the same redox system associated with acid–base equilibrium occurred, being this process well known for the redox mechanism of NF related to the electron-proton transfer process [26, 27, 35]. This behavior is an evidence of a probable fast protonation step preceding the charge transfer process [28] in which one proton participates in the rate-determining step of the reaction in the pH range studied whose involvement may have corresponded to a second slow protonation of the nitro group, subsequently reduced to the nitroso intermediate.

Tafel analysis (Figure 5D,E) was employed to probe the charge–transfer kinetics of nitrofurazone (NF) reduction using the relationship:
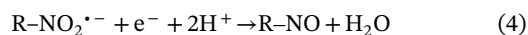
$$\alpha = \frac{RT \times dLn^I/I_{pc}}{F \times dE}$$

which R, T, F, and α represent the gas constant (8.314 J mol^{-1} K^{-1}), temperature (298 K), Faraday constant (96500 C), and charge–transfer coefficient, respectively. This approach assumes minimal reactant depletion at the electrode surface, ensuring diffusion-controlled NF concentration near the sensor interface [28, 36, 37].

This approach is valid as long as there has been little depletion of the reactant concentration, considering, in this case, the potential region in which the concentration of NF transported by diffusion

is close to the maximum at the sensor surface [28, 36, 37]. Thus, since the transfer coefficient values (α) are sensitive to the mechanism change in electrochemical processes, the Tafel slopes were obtained as shown on Table 4. It is worth highlighting that the region chosen in Figure 5D,E, reds bars, is the region where the process is controlled by kinetic. In this way, the evaluation of the potential range associated with the formation of hydroxylamine indicated that these results suggest that, at lower scan rates, the values are lower, but for MWCNT system the values are practically 2 times higher compared to the system with CuPc on the MWCNT matrix. However, at a higher scan rate, 400 mV s^{-1}, the charge transfer efficiency is increased in both systems, but the lower value is observed in the presence of CuPc in the MWCNT matrix. These observations indicates the electrocatalytic role of CuPc, probably facilitating a more efficient electron transfer process.

In alkaline medium, a distinct process can be observed with the appearance of a peak prior to $E_{pc,1}$, Figure 6A–C. The first reduction step cyclic voltammogram of NF at pH 10.04, $E_{pc,2}$, corresponds to the R-NO$_2$/R-NO$_2^{\bullet-}$ pair ((Equation (1)), with respective anodic component, $E_{pa,2}$. Therefore, under these conditions, a reversible reduction corresponds to (Equation (1)) involving one electron related to the R-NO$_2$/R-NO$_2^{\bullet-}$ couple and followed by the nitroso and hydroxylamine derivatives formation, as shown in Equations (4) and (5)).

$$R\text{–}NO_2^{\bullet-} + e^- + 2H^+ \rightarrow R\text{–}NO + H_2O \tag{4}$$

$$R\text{–}NO + 2e^- + 2H^+ \tag{5}$$

The NF voltammetric behavior registered for all electrode systems was similar. $I_{pc,1}$ value decreased approximately 10 times when compared to the acid medium, indicating smaller number of electrons involved. It is also noted that $E_{pc,1}$ value was shifted to more negative potential values when compared to the acid medium, with values of −0.75, −0.56, and −0.48 V being recorded GCE-C-MWCNT, GCE modified by C-MWCNT combined with CuPc and bare GCE, respectively. Furthermore, the NF voltammetric reduction regarding to the $E_{pc,2}$ and $E_{pa,2}$ values present a characteristic response for reversible processes, since the value of 90 mV for this difference (ΔE_p) remains constant as the scan rate increases at the GCE by C-MWCNT combined with CuPc, as well as observed for GCE-C-MWCNT [26] and GCE-C-MWCNT-Hemin [27]. With the aim of evaluating the R-NO$_2$/R-NO$_2^{\bullet-}$ redox couple from NF, cyclic voltammograms were adjusted to an appropriate potential range (0.2 V ≤ $E_{pc,2}$ ≤ −0.8 V) and recorded in a sufficiently alkaline media with NF 0.1 mmol L^{-1}, Figure 6D–F.

TABLE 4 | Experimental values of α obtained from the Tafel plot represent in Figure 5D,E at different scan rates. [NF] = 0.1 mmol L−1 at pH = 4.02.

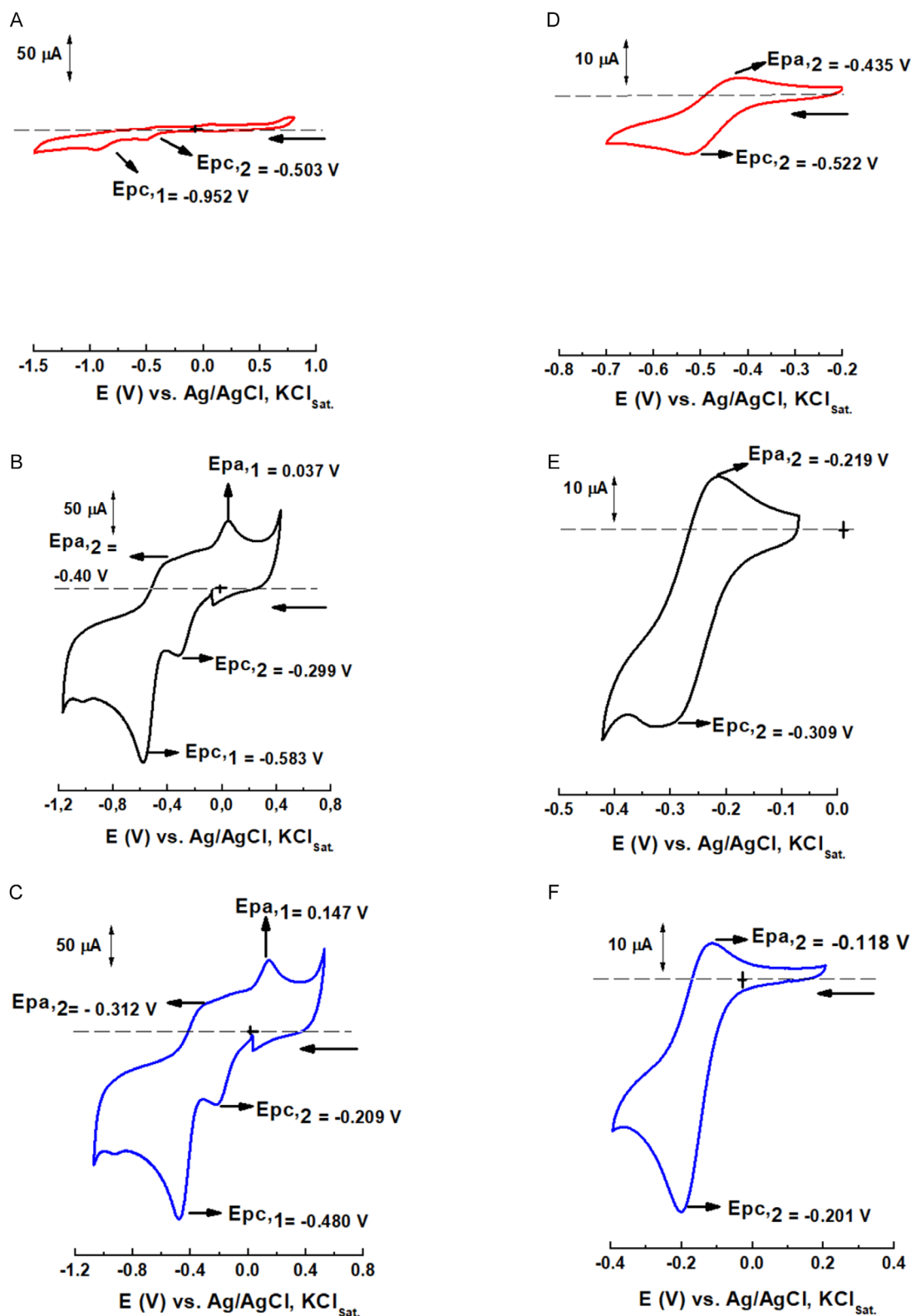| Scan rate, ν (V s^{-1})	α values (GCE-C-MWCNT-CuPc) (mol^{-1})	α values (GCE-C-MWCNT) (mol^{-1})
0.1	0.030	0.071
0.2	0.035	0.079
0.4	0.262	0.358

FIGURE 6 | Cyclic voltammograms (1st cycle): (A–C) hydroxylamine and nitro-anion radical between $-1.6\,V \leq E \leq 0.8\,V$ range, being (A) bare GCE, (B) GCE-C-MWCNT, (C) GCE modified by C-MWCNT combined with CuPc and (D–F) with only the nitro-anion radical record between $-0.8\,V \leq E \leq 0.4\,V$ range, being (D) bare GCE, (E) GCE-C-MWCNT, (F) GCE-C-MWCNT-CuPc. pH 10.04 phosphate buffer, $\nu = 200\,mV\,s^{-1}$.

An electrocatalytic effect can be noted for the NF reduction considering $E_{pc,2}$, since the potential was anticipated by approximately 100 and 290 mV compared with GCE-MWCNT and bare GCE, respectively. Additionally, the sensor with CuPc was also capable to anticipate $E_{pc,2}$ value in 130 mV when compared to the sensor with hemin [27]. Moreover, the current registered by the GCE modified by C-MWCNT combined with CuPc was increased 10 times in alkaline medium against the bare GCE

in the same order of magnitude to the GCE-C-MWCNT and GCE-C-MWCNT-HEMIN. It is possible to indicate that this increase in current may also be associated with an increase in surface area. This result is similar to the results obtained by Xia et al., who worked with graphene/CuPc to evaluate chloramphenicol, which is a nitroaromatic [38].

A comparison between the Randles–Ševčik [27, 39] slope values for GCE-C-MWCNT (7.44 $\mu A\ mVs^{-1/2}$) and the GCE-C-MWCNT combined with CuPc (8.15 $\mu A\ mVs^{-1/2}$) suggests that this latter presents a small gain in area compared with the former in order of 1.10 times, estimating an active area of 0.146 cm^2. Of course, the values of electrochemically active area are interdependent on factors intrinsic to all electrodes, such as roughness, heterogeneity, defects, and contours [39], suggesting that this value may be overestimated and does not unequivocally distinguish the catalytic effect of the nitro group regeneration as a reactant. In this way, according to the potential anticipation, in which the electrocatalytic cycle involves the electrochemical step of the nitro group reduction to the respective radical, being followed by the chemical step of the nitro group regeneration on the sensor surface with the participation of the Cu (II)/Cu (III) couple due to the presence of CuPc [38].

The superior electrocatalytic performance of the CuPc/C-MWCNT composite in alkaline media compared to acidic conditions is attributed to a pH-dependent mechanism involving copper redox states. Under alkaline conditions (pH > 9), hydroxyl ions promote the formation of Cu $(OH)_2$ on the CuPc surface, which is electrochemically oxidized to generate Cu (III) (CuOOH). This high-valent copper species acts as an electron-transfer mediator, facilitating the one-electron reduction of nitrofurazone (NF) to its nitro-anion radical (R-$NO_2^{\bullet-}$) and subsequently oxidizing the radical back to R-NO_2, enabling catalytic recycling of the Cu (II)/Cu (III) couple.

The absence of a distinct Cu (III) oxidation peak ($\sim$+0.56 V) in voltammetric profiles (Figures 5 and 6) likely arises from strong electronic interactions between CuPc's macrocyclic structure and the C-MWCNT matrix, which stabilize the Cu (III) intermediate and suppress its discrete electrochemical signature. In contrast, acidic media favor the persistence of Cu (II) as aquo/hydroxo complexes (e.g., [Cu $(H_2O)_6]^{2+}$), which lack the oxidative capacity to mediate radical recycling, resulting in reduced catalytic activity.

This behavior mirrors observations in copper-porphyrin systems, such as those reported by Bhaduri et al. [40] where Cu (III) intermediates in alkaline media drive catalytic cycles for non-enzymatic glucose oxidation. The planar CuPc macrocycle enhances π–π interactions with C-MWCNTs, promoting electron delocalization and interfacial charge transfer, while alkaline conditions lower the thermodynamic barrier for Cu (II) $\rightarrow$ Cu (III) oxidation.

These findings underscore the importance of electrolyte pH in tuning electrocatalytic pathways and highlight the CuPc/C-MWCNT system's ability to stabilize reactive intermediates for efficient nitrocompound detection. The insights gained here provide a foundation for designing adaptive catalytic interfaces with applications in pharmaceutical analysis and redox-mediated sensing.

3.4 | Interaction of the Radical Anion from NF with Glutathione, Cysteine, and Molecular Oxygen

According to previous results already observed during this work, the appearance of the R-NO_2/R-$NO_2^{\bullet-}$ redox couple for NF using the modified GCE modified by C-MWCNT combined with CuPc was recorded in alkaline media. For that reason, it was explored the reactivity of the radical towards aminothiols, which are endobiotic groups of vital importance to the biological environment, performing a similar function to oxygen and acting as scavengers of free radicals from active species [41–43]. According to some studies, there is a relevant reaction between the R-$NO_2^{\bullet-}$ and aminothiol compounds [35, 44, 45]. Cyclic voltammetry was used to evaluate the reactivity of the nitro-anion radical towards cysteine (Cys) and glutathione (GSH) in the potential range and scan rate in which the nitro-anion radical is detected. The complex electrochemical interactions in addition to electronical acceptors on the stability of R-$NO_2^{\bullet-}$ depend on the identities of the acceptor, the drug, the electrode surface and the supporting electrolyte concentration [45]. For that reason, this technique allows to identify the stability or reactivity of the reduction products, as reflected in relation to the peak currents, since it is possible to reduce or wipe out the formation of the hydroxylamine derivative [26]. Therefore, the interactions between R-$NO_2^{\bullet-}$ generated from NF were investigated with cysteine and glutathione on GCE modified by C-MWCNT combined with CuPc.

NF cyclic voltammograms recorded at pH 10.04 in the presence of different concentrations of Cys and GSH are shown in Figure 7A,B. It is possible to clearly observe that the aminothiols were very similar to each other referring to the $I_{pc,2}$, which does not undergo major changes even with the increase in the concentration of scavengers. However, the peaks corresponding to the hydroxylamine derivative ($I_{pc,1}$) significantly decreased 26% and 18% when 3.5 mmol L^{-1} of Cys and GSH were added, respectively. Moreover, respective drops of 30% and 40% were identified when 10.5 mmol L^{-1} Cys and GSH were employed. At the same time, the reversible radical oxidation showed a drop with the increase of concentration for both scavengers. It is possible to understand that Cys and GSH act in a similar and significant way as scavengers on the nitro-anion radical. Thus, the partial consumption of the radical compromised the derivatives subsequently generated. These results are compatible with those obtained with hemin as modifying agent [27] and similar with results registered by Fotouhi [45] and Julião [35], considering the reduction of the reoxidized peak derived from furazolidone on bare GCE and NF on HBDDE, respectively, for [aminothiol] $\leq 3.7 \times 10^{-2}$ mol L^{-1}, however with greater concentrations an adduct was formed. Therefore, the parameters such as concentration and electrode surface are significantly important in the reactivity of aminothiol compounds with the nitro-anion radical.

On the contrary, in Figure 7C, the radical behavior in the presence of oxygen is very different from that observed with aminothiol groups. $E_{pc,1}$ and $E_{pa,2}$ completely disappeared, showing that the R-$NO_2^{\bullet-}$ was quickly consumed. Molecular oxygen was added at a flow rate of 1 mL min^{-1} during 5 and 10 min at pH 10.04, following previous experience [46]. In sequence, a narrow potential range corresponding to the R-NO_2/R-$NO_2^{\bullet-}$ redox couple was selected (Figure 8D) specifically to observe the
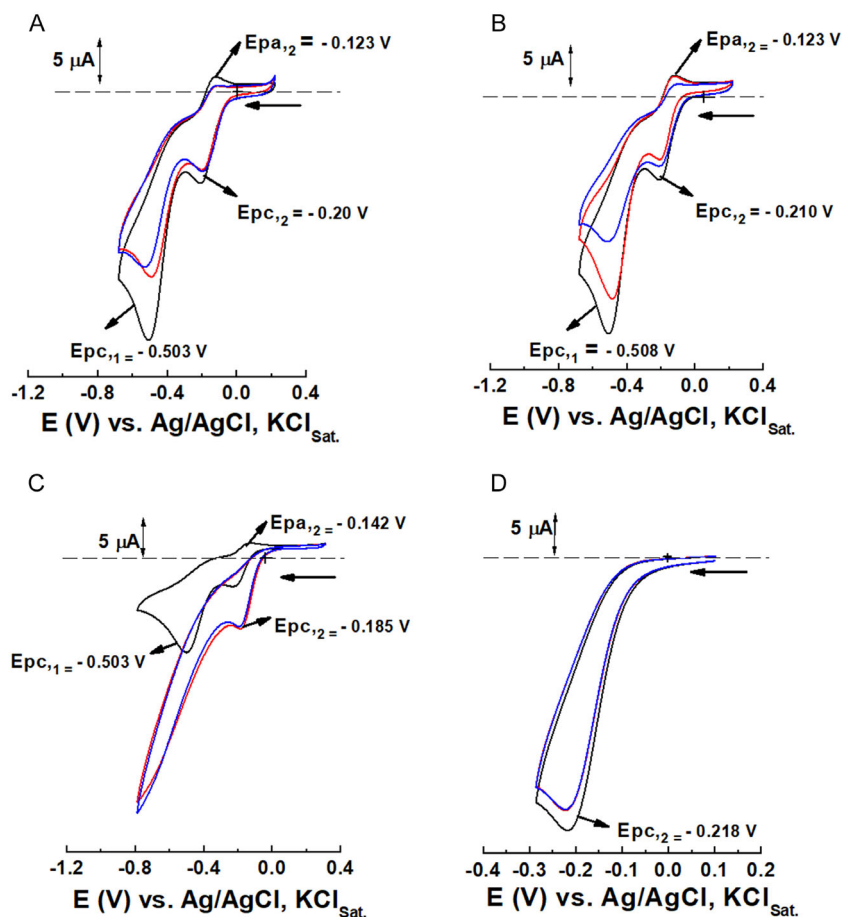
FIGURE 7 | Cyclic voltammograms recorded with GCE modified by C-MWCNT combined with CuPc adding (A) Cys and (B) GSH; being (black) absent of Cys and GSH; (red) 3.5 mmol L^{-1}; (blue) 10.5 mmol L^{-1}; (C) O$_2$ and (D) O$_2$ in a restricted potential range of 0.0 V $\leq E \leq -0.35$V. Flow flux of 1 mL min^{-1}, being (black) absent of O$_2$, (red) time of 5 min and (blue) time of 10 min with O$_2$. Phosphate buffer pH 10.04, [NF] = 0.1 mmol L^{-1} and $\nu = 200$ mV s^{-1}.

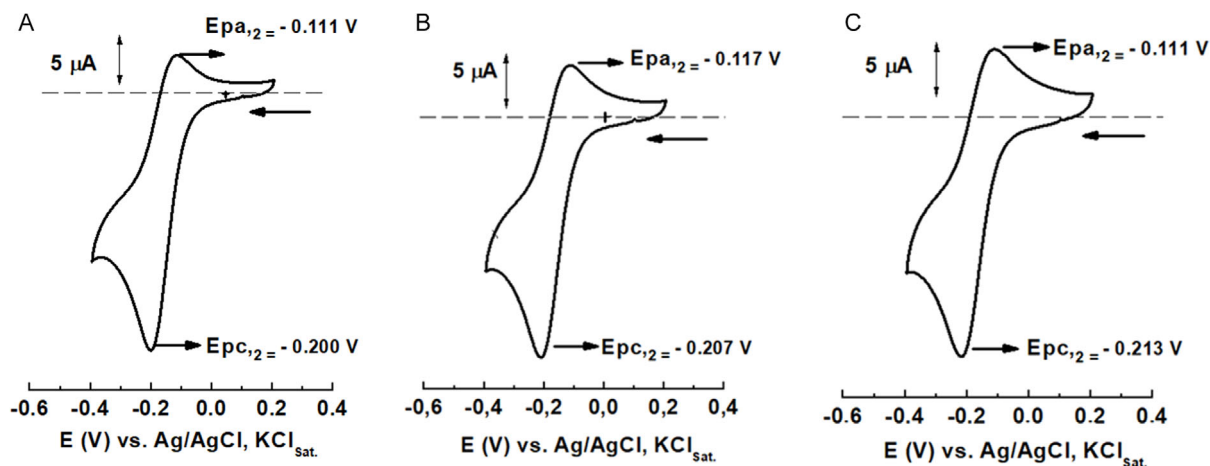**FIGURE 8** | Data obtained in phosphate buffer pH 10.04 with GCE modified by C-MWCNT combined with CuPc as working electrode, being (A) 0.1 Vs^{-1}, (B) 0.2 Vs^{-1}, and (C) 0.7 Vs^{-1}.

nitro-anion radical behavior in the oxygen presence. As it can be observed, the oxidation peak ($E_{pa,2}$) is completely absent. Therefore, the R-NO$_2$$^{•-}$ in aqueous medium and aerobic environment can transfer the one electron to O$_2$ producing the superoxide anion (O$_2$$^{•-}$), which is biologically active [46]. These results are similar to those obtained for nimorazole using bare GCE [46] and NF using GCE-C-MWCNT-HEMIN [27].

3.5 | Kinetic Stability of the Nitro-Anion Radical

Figure 8A–C shows the isolated register of the couple related to the nitro radical anion correspondent to the cyclic voltammograms of NF recorded at pH 10.04. The R-NO$_2$$^{•-}$ kinetic stability can be evaluated by applying a consolidated model using the current ratio ($I_{pc,2}/I_{pa,2}$) as electrochemical parameter [7, 26, 27, 35, 47, 48].

This model was developed by Olmstead-Nicholson [29] and according to data reported in the literature, the current ratio is dependent on pH, influenced by the scan rate and the concentration of the electroactive species. The scan rate effect and drug concentration on $I_{pc,2}/I_{pa,2}$ ratio are presented in Figure 9A,B employing GCE modified by C-MWCNT combined with CuPc. While the former shows that the current ratio tends to be close to the unity as the scan rate is increased, the latter shows that the current ratio decreases as the NF concentration increases. These diagnostic criteria fulfill the requirements for a coupled homogeneous electrode process, in which an irreversible chemical reaction follows a reversible charge–transfer step. Furthermore, this chemical irreversible reaction is considered second order [24]. This behavior is classic for nitrofurans [5, 26–28, 35, 48], describing that NF undergoes an irreversible reaction of disproportionation after the nitro-radical anion generation as described below:

$$2R-NO_2^{\bullet-} + 2H^+ \rightarrow R-NO_2 + R-NO + H_2O \quad (6)$$
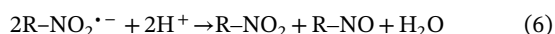
Taking this approach into account, the $I_{pc,2}/I_{pa,2}$ value experimentally obtained at each scan rate is interpolated into a working curve that determines the parameter ϖ, which incorporates the effects of the rate constant, nitroheterocyclic compound concentration and scan rate [29]. Figure 10 shows the plots in which the kinetic parameters (ϖ as a function of τ) obtained with GCE-C-MWCNT-CuPc present linear relationships. Table 5 brings the respective k_2 and $t_{1/2}$ values referents to the presence and absence of radical scavengers. The lifetime determination of drugs with biological activity in aqueous media can be an important parameter to be considered in quantitative studies of the relationship between chemical structure and biological activity, especially considering that the intracellular environment is predominantly aqueous [27]. From these data, the highest k_2 values for both systems with molecular oxygen application were observed, indicating lower radical stability and the oxygen presence showed the best performance as radical acceptor comparing to the aminothiols. Nevertheless, as radical acceptors GSH and Cys presented results practically no significant change in $t_{1/2}$ when compared to bare GCE. Thus, these results suggest that under aerobic conditions the radical is transferred to molecular oxygen and produces superoxide $O_2^{\bullet-}$, which is biologically active, as already indicated in (Reaction 2).

FIGURE 10 | Relationship between ϖ and τ with presence of (■) oxygen, (▼) GSH, (●) Cys, and (▲) without scavenger. Data obtained in phosphate buffer pH 10.04, [NF] = 0.1 mmol L^{-1}; scan rate between 50 and 700 mV s^{-1}; GCE modified by C-MWCNT combined with CuPc as working electrode.

TABLE 5 | The k_2 and $t_{1/2}$ values for the nitro-radical anion disproportionation reaction and the radical scavenger actions. [NF] = 0.1 mmol L−1 at pH = 10.04.

Sensor	Scavenger	$k_2 \times 10^{-3}$ (L mol^{-1}s^{-1})	$t_{1/2}$ (s)
Bare GCE	—	22.60	0.44
GCE-C-MWCNT	—	12.86	0.78
GCE modified by C-MWCNT combined with CuPc	—	12.28	0.81
	*O$_2$	29.00	0.34
	**GSH	24.96	0.40
	**Cys	21.72	0.41

Note: (*) O$_2$ flow flux of 1 mL/min; (**) [GSH] = [Cys]: 3.5 mmol L^{-1}.

Nonetheless, comparing the system with CuPc against bare GCE there was an increase in stability, since $t_{1/2}$ value is approximately 2.0 times higher. Furthermore, it was observed that the
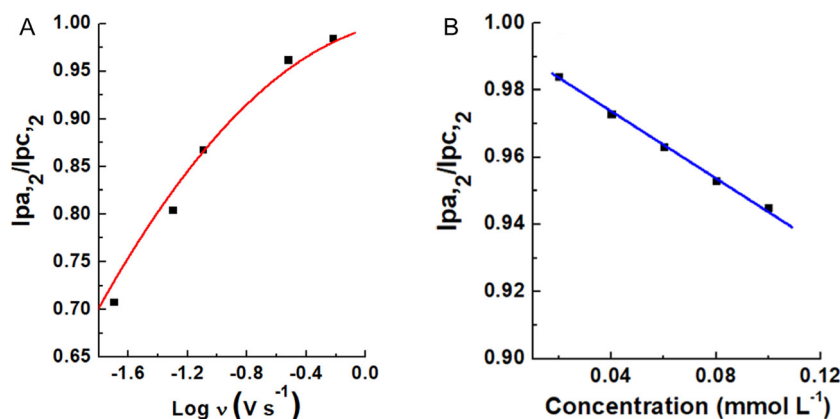

FIGURE 9 | (A) Relationship between the $I_{pa,2}/I_{pc,2}$ ratios and log ν, data obtained in phosphate buffer pH 10.04, being the interval of scan rate, $0.02 \le \nu \le 0.7$ Vs^{-1} with [NF] = 0.1 mmol L^{-1}; (B) relationship between $I_{pa,2}/I_{pc,2}$ ratios and NF concentration with $\nu = 200$ mV s^{-1}.
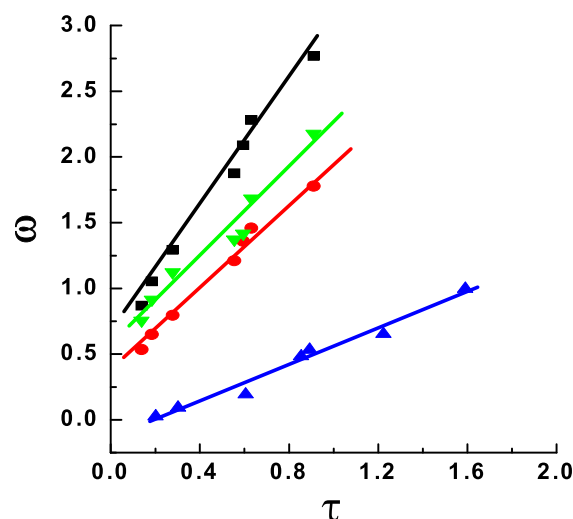
nitro-radical anion stability was similar between GCE-C-MWCNT and GCE-C-MWCNT combined with CuPc, being $t_{1/2}$ values 0.78 s and 0.81 s, respectively. Although the gain in the radical stability is low, this small difference corroborates the biological model of enzymatic interaction involving nitroheterocyclic drugs, corroborating previous results having hemin as modifier agent [27, 49]. In this sense, this result is interesting from a biological point of view, since phthalocyanines, Pcs (CuPc, of this work) is structurally similar to the enzymes of the P450 reductase complex [17, 18, 48].

4 | Conclusion

SEM and FTIR analyses confirmed that the CuPc/C-MWCNT composite achieves stability through electrostatic interactions between amino/Cu (II) groups in CuPc and carboxylic moieties on C-MWCNTs. This interaction creates a conductive matrix that enhances voltammetric signals for nitrofurazone (NF) reduction intermediates, particularly hydroxylamine derivatives and the nitro-anion radical (R-NO$_2^{\bullet-}$). The CuPc/C-MWCNT-modified GCE demonstrated a 290 mV reduction in overpotential for R-NO$_2^{\bullet-}$ formation compared to bare GCE and 100 mV vs. GCE-C-MWCNT, highlighting CuPc's role in lowering activation barriers. Cathodic currents increased ~10-fold in alkaline media relative to bare GCE, with comparable magnitudes to GCE-C-MWCNT, indicating improved electron transfer kinetics.

Molecular oxygen (O_2) was identified as the dominant scavenger of R-NO$_2^{\bullet-}$, regenerating NF via a one-electron pathway to produce superoxide anion ($O_2^{\bullet-}$). This contrasts with aminothiols (Cys, GSH), which showed minimal scavenging activity. The CuPc/C-MWCNT interface exhibited structural stability across electrochemical cycles, attributed to strong π–π stacking and electrostatic interactions, enabling precise determination of radical half-lives via cyclic voltammetry.

The synergy between CuPc's redox-active macrocycle and C-MWCNT's conductivity facilitates extended radical lifetimes and pH-dependent catalysis. Alkaline conditions promote Cu (OH)$_2$/Cu (III) mediation, while acidic media limit catalytic pathways. This methodology offers sub-micromolar sensitivity, reproducibility, and adaptability to other nitroheterocyclic drugs, linking radical stability to bioactivity.

The CuPc/C-MWCNT system bridges material science and electroanalytical chemistry, providing a low-cost platform to study nitrocompound mechanisms and advance drug quality control. Its ability to resolve short-lived radicals and correlate lifetimes with therapeutic efficacy positions it as a critical tool for pharmaceutical research.

Author Contributions

Charles L. Brito: conception and design of study, acquisition of data, analysis and/or interpretation of data, drafting the manuscript. **Elizabeth I. Ferreira**: revising the manuscript critically for important intellectual content. **Mauro A. La-Scalea**: revising the manuscript critically for important intellectual content.

Conflicts of Interest

The authors declare no conflicts of interest.

Data Availability Statement

The data that support the findings of this study are available from the corresponding author upon reasonable request.

References

1. S. T. Abreu, L. G. V. Gelves, E. J. Barreiro, and L. M. Lima, "Revisting Nitroaromatic Drugs: Mechanisms of Bioactivation, Metabolism and Toxicity and Methods to Synthesize Nitroaromatic Fragments," *Journal of the Brazilian Chemical Society* 35 (2024): 1–34, https://doi.org/10.21577/0103-5053.20240071.

2. D. G. G. Rando, H. G. O. Costa, T. F. Heitor, J. de Moraes, T. F. A. Pavani, and Employing, "Red Flags, to Fight the Most Neglected Diseases: Nitroaromatic as Still Suitable Tools to Treat Human and Veterinary Parasitosis," *Current Topics in Medicinal Chemistry* 23 (2023): 816–832, https://doi.org/10.2174/1568026623666230427114840.

3. O. Hammerich, "Organic Electrochemistry: Revised and Expanded," *CRC Press* 5, no. 30 (2015): 1149–1200, https://doi.org/10.1201/b19122.

4. C. Lema, R. Moscoso A. A.-Lueje, and J. Squella, "Electrochemical Nicarbazin Analysis: Rapid Determination on Bucky Paper Disks Constructed from MWCNT," *Journal of the Electrochemical Society* 171 (2024): 066503, https://doi.org/10.1149/1945-7111/ad541a.

5. S. Bollo, L. J. Nunez-Vergara, C. Martinez, G. Chauviere, J. Perie and J. A. Squella, "Voltammetric study of nitro-radical anion generated from nitrofuran compounds of pharmacological significance," *Electroanalysis* 15 (2003): 9–25, https://doi.org/10.1002/elan.200390000.

6. J. A. Squella, S. Bollo, and L. J. Nuñez-Vergara, "Recent Developments in the Electrochemistry of Some Nitro Compounds of Biological Significance," *Current Organic Chemistry* 9 (2005): 565–581, https://doi.org/10.2174/1385272053544380.

7. T. Symons, J. H. Tocher, D. A. Tocher, and I. Edwards, "Electrochemical Studies of Nitroheterocyclic Compounds of Biological Interest VII. Effect of Electrode Material," *Free Radical Research Communications* 14 (1991): 33–40, https://doi.org/10.3109/10715769109088939.

8. P. C. Mandal, "Reactions of the Nitro Radical Anion of Metronidazole in Aqueous and Mixed Solvent: A Cyclic Voltammetric Study," *Journal of Electroanalytical Chemistry* 570 (2004): 55–61, https://doi.org/10.1016/j.jelechem.2004.02.030.

9. C. G. Sanz, K. A. Dias, R. P. Bacil, et al., "Electrochemical Characterization of Para- and Meta-Nitro Substituents in Aqueous Media of New Antichagasic Pharmaceutical Leaders," *Electrochimica Acta* 368 (2021): 137582, https://doi.org/10.1016/j.electacta.2020.137582.

10. T. S. Lima, M. O. Almeida, M. A. La Scalea, K. M. Honorio, M. C. Santos, and L. Codognoto, "Diamond Electrodes Applied to the Voltammetric Generation of Nitro-Anion Radicals from Methyl

Parathion in Aqueous Media," *Diamond and Related Materials* 110 (2020): 108112, https://doi.org/10.1016/j.diamond.2020.108112.

11. R. Peng, A. Offenhausser, Y. Ermolenki, and Y. Mourzina, "Biomimetic Sensor Based on Mn (III) *Meso*-Tetra(N-Methyl-4-Pyridyl) Porphyrin for Non-Enzymatic Electrocatalytic Determination of Hydrogen Peroxide and as an Electrochemical Transducer in Oxidase Biosensor for Analysis of Biological Media," *Sensors and Actuators B: Chemical* 321 (2020): 128437, https://doi.org/10.1016/j.snb.2020.128437.

12. V. Erady, R. J. Mascarenhas, A. K. Satpati, A. K. Bhakta, Z. Mekhalif, and J. Delhalle, "Sensitive Voltammetric Determination of Morin in *Psidium Guajava* Leaf Extract at Nickel (II) Phthalocyanine Modified Carbon Paste Electrode," *Surfaces and Interfaces* 19 (2020): 100517, https://doi.org/10.1016/j.surfin.2020.100517.

13. B. S. Jilani, M. P. Malathesh, C. D. Mruthyunjayachaari, and K. R. V. Reddy, "Cobalt (II) Tetra Methyl-Quinoline Oxy-Bridged Phthalocyanine Carbon Nano Particles Modified Glassy Carbon Electrode for Sensing Nitrite: A Voltammetric Study," *Materials Chemistry and Physics* 239 (2020): 121920, https://doi.org/10.1016/j.matchemphys.2019.121920.

14. R. F. Nascimento, T. M. G. Selva, W. F. Ribeiro, M. F. Belian, L. Agnes, and V. B. Nascimento, "Flow-Injection Electrochemical Determination of Citric Acid Using a Cobalt (II)–phthalocyanine Modified Carbon Paste Electrode," *Talanta* 105 (2013): 354–359, https://doi.org/10.1016/j.talanta.2012.10.055.

15. K. M. Kadish, K. M. Smith, and R. Guilards, The Porphyrin Handbook- Applications of Phthalocyanines, (Academic Press New York, 2003).

16. S. Yang, S. Yu, X. Gao, Z. Zhang, and F. Wang, "Recent Advances in Electrocatalysis with Phthalocyanines," *Chemical Society Reviews* 50 (2021): 12985–13011, https://doi.org/10.1039/D0CS01605E.

17. A. C. Boni, A. Wong, R. A. F. Dutra, and M. D. P. T. Sotomayor, Cobalt Phthalocyanine as a Biomimetic Catalyst in the Amperometric Quantification of Dipyrone Using FIA," *Talanta* 85 (2011): 2067–2073, https://doi.org/10.1016/j.talanta.2011.07.038.

18. A. Wong, M. R. V. Lanza, and M. D. P. T. Sotomayor, "Sensor for Diuron Quantitation Based on the P450 Biomimetic Catalyst Nickel (II) 1,4,8,11,15,18,22,28-Octabutoxy-29H,31H-Phthalocyanine," *Journal of Electroanalytical Chemistry* 690 (2013): 83–88, https://doi.org/10.1016/j.jelechem.2012.11.007.

19. Y. Gu, X. Yan, C. Li, et al., "Biomimetic Sensor Based on Molecularly Imprinted Polymer with Nitro Reductase –like Activity for Metronidazole Detection," *Biosensors and Bioelectronics* 77 (2016): 393–399, https://doi.org/10.1016/j.bios.2015.09.060.

20. B. Halliwell and J. M. C. Gutteridge, Free Radical in Biology and Medicine, 4th ed. (Oxford, 2007).

21. Z. Y. Cai, L. Z. Pei, Y. Yang, Y. Q. Pei, C. G. Fan, and D. F. Fu, "Electrochemical Behavior of Tartaric Acid at CuGeO3 Nanowire Modified Glassy Carbon Electrode," *Journal of Solid State Electrochemistry* 16 (2012): 2243–2249, https://doi.org/10.1007/s10008-012-1654-2.

22. K. Borsos and G. Inzelt, "Electrochemical and Nanogravimetric Studies of Poly (copper Phthalocyanine) Microparticles Immobilized on Gold in Aqueous Solutions," *Journal of Solid State Electrochemistry* 19 (2015): 2565–2577, https://doi.org/10.1007/s10008-015-2770-6.

23. S. Arslan and I. Yilmaz, "Preparation, Electrochemical, and Spectroelectrochemical Characterization of a New Water-Soluble Copper Phthalocyanine," *Inorganic Chemistry Communications* 10 (2007): 385–388, https://doi.org/10.1016/j.inoche.2006.12.004.

24. M. Arıcı, D. Arıcan, A. L. Uğur, A. Erdoğmuş, and A. Koca, "Electrochemical and Spectroelectrochemical Characterization of Newly Synthesized Manganese, Cobalt, Iron and Copper Phthalocyanines," *Electrochimica Acta* 87 (2013): 554–566, https://doi.org/10.1016/j.electacta.2012.09.045.

25. J. Lurie, Handbook of Analytical Chemistry (Mir, 1978), 488p.

26. C. L. Brito, E. I. Ferreira, and M. A. La-Scalea, "Multi-Walled Carbon Nanotube Functionalization and the Dispersing Agents Study Applied for the Glassy Carbon Electrode Modification and Voltammetric Reduction of Nitrofurazone," *Journal of Solid State Electrochemistry* 24 (2020): 1969–1980, https://doi.org/10.1007/s10008-020-04621-2.

27. C. L. Brito, E. I. Ferreira, and M. A. La-Scalea, "Application of Multi-Walled Carbon Nanotubes Functionalized with Hemin to Evaluate the Electrochemical Behavior of Nitrofurazone in Aqueous Media," *Electrochimica Acta* 459 (2023): 142486, https://doi.org/10.1016/j.electacta.2023.142486459.

28. C. B.-McAuley, E. Kätelhçn, E. O. Barnes, R. G. Compton, E. Laborda, and A. Molina, "Recent Advances in Voltammetry," *ChemistryOpen* 4 (2015): 224–260, https://doi.org/10.1002/open.201500042.

29. J. D. Mozo, J. Carbajo, J. C. Sturn, L. J. Nuñez-Vergara, R. Moscoso, and J. A. Squella, "The use of Digital Simulation to Improve the Cyclic Voltammetric Determination or Rate Constants for Homogeneous Chemical Reactions following Charge Transfers," *Analytica Chimica Acta* 699 (2011): 33–43, https://doi.org/10.1016/j.aca.2011.04.060.

30. E. T. Saka, H. Yalazan, Z. Bryikioglu, H. Kantekin, and K. Tekintas, "Synthesis, Aggregation, Photocatalytical and Electrochemical Properties of Axially 1-Benzylpiperidin-4-Oxy Units Substituted Silicon Phthalocyanine," *Journal of Molecular Structure* 1199 (2020): 126944, https://doi.org/10.1016/j.molstruc.2019.126994.

31. Y. Yamada, T. Sugiura, K. Morita, H. Ariga-Miwa, and K. Tanaka, "Improved Synthesis of Monocationic μ– Nitrido-Bridged Iron Phthalocyanine Dimer with No Peripheral Substituents," *Inorganica Chimica Acta* 489 (2019): 160–163, https://doi.org/10.1016/j.ica.2019.02.021.

32. R. M. Silverstein, F. X. Webster, and D. Kiemle, Spectrometric Identification of Organic Compounds, 8th ed. (Wiley, 2014).

33. H. Li, Z. Zu, H. Li, et al., "Modification of Multi-Walled Carbon Nanotube with Cobalt Phthalocyanine: Effects of the Templates on the Assemblies," *Journal of Materials Chemistry* 21 (2011): 1181–1186, https://doi.org/10.1039/C0JM02156C.

34. M.-E. Stogia, A.-E. Dimou, G. Maistros, and N. D. Alexopoulos, "Investigation of Multi-Walled Carbon Nanotubes Aqueous Dispersions via Electrical Impedance Spectroscopy," *Materials Today: Proceedings* 93 (2023): 779–784, https://doi.org/10.1016/j.matpr.2023.07.040.

35. M. S. S. Julião, E. I. Ferreira, N. G. Ferreira, and S. H. P. Serrano, "Voltammetric Detection of the Interactions between RNO_2 and Electron Acceptors in Aqueous Medium at Highly Boron Doped Diamond Electrode (HBDDE)," *Electrochimica Acta* 51 (2006): 5080–5086, https://doi.org/10.1016/j.electacta.2006.03.054.

36. W. Wu, Q. Lu, G. Li, and Y. Wang, "How to Extract Kinectic Information from Tafel Analysis in Electrocatalysis," *Journal of Chemical Physics* 159 (2023): 221501, https://doi.org/10.1063/5.0175156.

37. R. P. Bacil, P. H. M. Garcia, W. R. Araujo, and S. H. P. Serrano, "Mechanism and Kinetics of Olanzapine and Quetiapine Oxidations at Glassy Carbono Electrode," *Electrochimica Acta* 368 (2021): 137683, https://doi.org/10.1016/j.electacta.2020.137683.

38. Y.-M. Xia, W. Zhang, M.-Y. Li, M. Xia, L.-J. Zou, and W.-W. Gao, "Effective Electrochemical Determination of Chloramphenicol and Florfenicol Based on Graphene/Copper Phthalocyanine Nanocomposites Modified Glassy Carbon Electrode," *Journal of the Electrochemical Society* 166 (2019): B654–B663, https://doi.org/10.1149/2.0801908jes.

39. D. Coelho, G. M. Luiz, and S. A. S. Machado, "Estimating the Electrochemically Active Area: Revisiting a Basic Concept in Electrochemistry," *Journal of the Brazilian Chemical Society* 32 (2021): 1912–1917, https://doi.org/10.21577/0103-5053.20210080.

40. S. N. Bhaduri, D. Gosh, S. Debnath, R. Biswas, and P. B. Chatterjee, "Cooper (II) Incorporated Porphyrin-Based Porous Organic Polymer for

Anonenzymatic Electrochemical Glucose Sensor," *Inorganic Chemistry* 62 (2023): 4136–4146, https://doi.org/10.1021/acs.

41. P. Mlejnek, "Direct Interaction between N-Acetylcysteine and Cytotoxic Electrophile - an Overlooked in Vitro Mechanism of Protection," *Antioxidants* 11 (2022): 1485, https://doi.org/10.3390/antiox11081485.

42. M. Vairetti, L. G. Di Pasqua, M. Cagna, P. Richelmi, A. Ferrigno, and C. Berardo, "Changes in Glutathione Content in Liver Diseases: An Update," *Antioxidants* 10 (2021): 364, https://doi.org/10.3390/antiox10030364.

43. K. Ulrich and U. Jakob, "The Role of Thiols in Antioxidant Systems," *Free Radical Biology and Medicine* 140 (2019): 14–27, https://doi.org/10.1016/j.freeradbiomed.2019.05.035.

44. C. M. Aravena, A. C. Olea, H. Cerecetto, M. Gonzalez, J. Diego Maya, and J. Rodriguez-Becerra, "Potent 5-Nitrofuran Derivatives Inhibitors of *Trypanosoma Cruzi* Growth: Electrochemical, Spectroscopic and Biological Studies," *Spectrochimica Acta Part A: Molecular and Biomolecular Spectroscopy* 79 (2011): 312–319, https://doi.org/10.1016/j.saa.2011.02.007.

45. L. Fotouhi and S. Faramarzi, "Voltammetric Studies on Nitro Radical Anion Formation from Furazolidone and Kinetic of the Coupled Chemical Reaction," *Journal of Electroanalytical Chemistry* 568 (2004): 93–99, https://doi.org/10.1016/j.jelechem.2004.01.009.

46. C. L. Brito, R. S. O. Lins, M. Bertotti, E. I. Ferreira, and M. A. La-Scalea, "Free Radical Formation Evidence from Nimorazole Electrochemical Reduction in Aqueous Media," *Electrochimica Acta* 403 (2022): 139709, https://doi.org/10.1016/j.electacta.2021.139709.

47. M. P. Murphy, A. Holmgren, N. G. Larsson, et al., "Unraveling the Biological Roles of Reactive Oxygen Species," *Cell Metabolism* 13 (2011): 361–366, https://doi.org/10.1016/j.cmet.2011.03.010.

48. J. A. Squella, M. E. Letelier, L. Lindermeyer, and L. J. Nuñes-Vergara, "Redox Behavior of Nifuroxazide: Generation of the One-Electron Reduction Product," *Chemico-Biological Interactions* 99 (1996): 227–238, https://doi.org/10.1016/0009-2797(95)03672-5.

49. V. Amendola, C. Dallacosta, L. Fabbrizzi, and E. Monzani, "A Hybrid Molecular Machine," *Tetrahedron* 64 (2008): 8318–8323, https://doi.org/10.1016/j.tet.2008.05.041.